Detection, Estimation and Correction of Faraday Rotation in Linearly Polarized SAR Backscatter Signatures

Anthony Freeman, Sasan S. Saatchi
Jet Propulsion Laboratory
California Institute of Technology
4800 Oak Grove Drive
Pasadena, California 91109

Y. Kuga and A. Ishimaru,
University of Washington,
Seattle, Washington

Abstract. The effect of Faraday rotation on linearly polarized backscatter measurements from space is addressed. Single-polarized, dual-polarized and quad-polarized backscatter measurements subject to Faraday rotation are first modeled, then the impacts are assessed using L-Band and P-Band polarimetric SAR data. It is shown that due to Faraday rotation, the received signal includes other polarization characteristics of the surface, which may be detectable under certain conditions. Techniques are developed to detect the presence of Faraday rotation in dual-polarized and quad-polarized SAR data. A novel approach to estimate the Faraday rotation angle Ω directly from linearly polarized SAR backscatter data is presented. Subsequent correction (or calibration) of fully polarimetric data for Faraday rotation, to recover the true scattering matrix, is described. This technique can be applied to the measured polarization signature of any scatterer and removes a key obstacle to the deployment of longer wavelength SARs (e.g. a P-Band SAR) in space. In the case of scatterers which have non-zero cross-polarized returns, it is shown that a potential $\pi/2$ ambiguity in Ω can be removed. Based on the technique to recover Ω, a new approach for measuring total electron content (TEC) from low earth orbit is suggested, which may provide high spatial resolution maps of TEC, over areas not presently covered by ground-based instrumentation.

Introduction

It has long been known that radio waves passing through the ionosphere may be subject to Faraday rotation, in which a linearly polarized wave has its plane of polarization rotated as it propagates through the plasma, e.g. [*Thompson et al*, 1986]. The magnitude of this effect depends on the radio frequency, the electron density along the path of propagation, the flux density of the Earth's magnetic field, and the angle of the wave propagation direction with respect to the direction of the magnetic field vector. After [*Evans and Hagfors*, 1968], the Faraday rotation angle may be many multiples of 2π for HF frequencies when the electron density is maximum. The degree of Faraday rotation is proportional to the inverse square of the frequency so that the effects of Faraday rotation can usually be ignored for radio frequencies above 1-2 GHz, but may be significant at lower frequencies, such as P-Band (~400 MHz). Under certain circumstances, e.g. observations made at midday during solar maximum, Faraday rotation may be a significant problem at L-Band (~1.2 GHz).

Measurement of Faraday rotation using a ground-based antenna to receive VHF signals of known polarization generated by a geostationary satellite, was first reported by [*Garriott et al*, 1965]. Such measurements can be used to estimate Total Electron Content for the ionosphere at the location of the ground receiving station, using the method of [*Titheridge*, 1972]. The utilization of these 'Faraday polarimeters' requires a suitably located geostationary satellite, generating the required signals at known frequency/polarization, and intensive observations using dedicated ground equipment and personnel. When available, these measurements offer key insights into transient, large-scale ionospheric phenomena [e.g. *Daniell et al*, 1996]

The effect of Faraday rotation on measurements of the polarization scattering matrix using monostatic radars was first addressed by [*Bickel and Bates*, 1965], who formulated the relation between measured and actual scattering matrices and showed that Faraday rotation is a non-reciprocal effect. The authors introduced an approach to calibrate polarimetric measurements subject to Faraday rotation using a calibration target such as a sphere or trihedral corner reflector, which has no cross-polarized return. They also described an approach to estimate and remove the effect of Faraday rotation from the measured scattering matrix of an arbitrary scatterer. This was done by referencing the measured scattering matrix to circular polarization: the result is an estimate for the Faraday rotation angle modulo $\pi/2$.

[*Gail*, 1993] formulated a system model which combined the effects of Faraday rotation and system errors such as antenna cross-talk and transmit/receive gain and phase imbalances. This author also described a numerical approach to calibration of measurements subject to such errors, but in [*Gail*, 1998] calls for a more robust approach to calibration of polarimetric radar measurements subject to Faraday rotation. The latter paper also addressed the effect of Faraday rotation on synthetic aperture radar (SAR) backscatter measurements at scale lengths smaller than the synthetic aperture length, concluding that, for most cases of interest this could be ignored. This result was confirmed by [*Rosen*, 1992] and [*Kutuza et al*, 1996].

Other ionospheric effects on radio propagation include absorption, which is negligible at UHF (and above) [*Chu and Lenzing*, 1991], except under rare conditions in the auroral or polar regions, when it may reach 1 or 2 dB. Refraction should also be negligible, according to [*Thompson et al*, 1986]. For SAR measurements, the coherence length of the ionosphere may limit the achievable spatial resolution in azimuth, at frequencies less than or equal to 1 GHz [*Quegan and Lamont*, 1986] and [*Ishimaru, Kuga and Liu*, 1997]. Path length delays may shift the backscatter returns from their 'true' positions. In what follows, it shall be assumed that the spatial resolution and sampling have been chosen so that resolution broadening in azimuth and shifts caused by group delay can be ignored. Path length delays may also yield large phase offsets at low frequencies, which may cause problems in comparing phase measurements from successive observations, for example as in repeat-pass interferometry. The standard approach to correct such phase problems caused by ionospheric delay is to combine measurements at two widely separated frequencies [*Thompson et al*, 1986]. In polarimetric measurements, this type of phase error does not usually impact the measurements, since only relative phases between polarizations (which are measured at the same time) are of interest. It is assumed here that the differences between path lengths at H and V can be ignored for near-simultaneous measurements.

Since 1988, NASA/JPL have been operating a P-Band SAR from a DC-8 airborne platform, as part of the AIRSAR set of instruments. The calibrated, polarimetric measurements made by the P-Band SAR have been used by earth scientists all over the world in a variety of disciplines. Amongst the most important results stemming from this activity are the noted strong correlation between linearly polarized backscatter measurements made at P-Band and above-ground, dry woody biomass for a variety of forest types [e.g. *Dobson et al*, 1992, *LeToan et al*, 1992, *Rignot et al*, 1995] . Others have pointed to the usefulness of P-Band backscatter measurements in monitoring forest inundation, mapping subtropical forests and wetlands, measuring ice sheet thickness and bathymetry of coastal areas [*Evans (ed.)* , 1995]. It is clear from these results that a P-Band

spaceborne SAR could provide useful data for several earth science disciplines. Faraday rotation is a significant obstacle to the deployment of longer wavelength (i.e. $\lambda > 30$ cm) spaceborne SARs for geophysical applications, and may even affect observations made by L-Band SARs, such as the Japanese Space Agency's JERS-1 or NASA's planned LightSAR system. Without a viable solution to this problem, backscatter measurements made by longer wavelength SARs will be difficult if not impossible to calibrate, which will mean that they will not be useful in most geophysical algorithms which use radar measurements. Before a spaceborne P-Band SAR can be flown, then, the potential problem of Faraday rotation must be resolved, which is the main thrust of this paper.

Ionospheric Effects

The ionosphere is defined to be the region of the upper atmosphere with large quantities of charged particles (an ionized medium). This ionized medium becomes anisotropic in the presence of a steady magnetic field such as the Earth's magnetic field. Radio waves propagating through the ionosphere therefore experience a rotation of polarization vector known as Faraday's rotation. The magnitude of the Faraday rotation angle depends on the frequency of the wave, the direction of the earth's magnetic field and its plasma electron density. Since the parameters of the earth's ionosphere are dynamic and their fluctuations depend on diurnal, seasonal, latitudinal and solar cycle effects, accurate prediction of the Faraday rotation of the polarization vectors is difficult. Therefore, we use the nominal values of electron density at the frequency of operation and the magnitude of the earth's magnetic field assuming a vertically homogenous ionosphere model.

After [*Titheridge*, 1972], the Faraday rotation angle of a linearly polarized electromagnetic wave of frequency f, which has traveled from a height h_s through the ionosphere is given by:

$$\Omega = \frac{K}{f^2} \int_0^{h_s} N B \cos\theta \sec\chi \, dh \tag{1}$$

where Ω is the total Faraday rotation angle for the signal, K is a constant (equal to 2.36 x 10^4 in mks units), N is the electron density (in m^{-3}), B is the magnetic flux density, θ is the angle between the ray path and the direction of the magnetic field, and χ is the angle between the ray path and the vertical. It is customary to take a weighted mean value of the 'magnetic field factor' ($B \cos\theta \sec\chi$), which is approximately equal to its value at 400 km [*Garriott et al*, 1965]. Equation (1) then becomes:

$$\Omega = \frac{K}{f^2} \overline{B \cos\theta \sec\chi} \, I_s \tag{2}$$

where

$$I_s = \int_0^{h_s} N \, dh$$

I_s is the integrated electron content up to the height h_s, sometimes referred to as the Total Electron Content, or TEC, for large h_s.

Equation (1) is valid under the quasi-parallel condition when the operating frequency is greater than both the plasma and the gyro frequencies and θ is not close to $\pi/2$ [*Yeh and Liu*, 1972]. The variables B and N depend on several dynamic parameters of the ionosphere as mentioned earlier. The distribution of these parameters along the propagation path are difficult to determine. Maximum electron densities are found in temperate latitudes and in winter during the midday. In regions near the geographic equator at about an angle 150 degrees from the magnetic equator the electron density is smaller. From the literature, the electron density also varies with respect to the height, reaching its maximum at between 300 to 400 km within the F2 region of the ionosphere [*Evans and Hagfors*, 1968].

The maximum value of the electron density for different latitudes can be obtained by employing the critical frequency of the ionosphere (maximum plasma frequency) in the following expression:

$$N = 1.24 f_c^2 \times 10^{10} \tag{3}$$

The critical frequency f_c can be derived from measurements and ionization maps that are often made for each hour of each month and for both solar minimum and maximum. Equation (3) is employed to derive the limiting cases for electron density of the ionosphere. Inserting the above expression for N into equation (2), the Faraday rotation angle Ω can be calculated assuming that the electron density is constant along the path. Therefore, the limiting cases are used to calculate the range of Faraday rotation of the received signal for a satellite at h_s = 568 km altitude and midday observations. The angle between the Earth magnetic field and the direction of propagation will be approximated constant at $\theta = 51.5^o$ = (90.0 -38.5°), consistent with a typical viewing angle for a spaceborne SAR.

Table 1 provides the limiting cases of the Faraday rotation angle in degrees for regions at about $\pm 15^o$ from the equator, as viewed by a satellite at 568 km, with a look angle of ~38.5 degrees. The calculations are performed for both midday and midnight. The table shows that Faraday rotation may be significant for L-Band and P-Band spaceborne SARs, but not for C-Band. The calculated values of integrated electron content given in Table 1 were arrived at by assuming the electron density N to be constant at the maximum value given in the table over the entire path to the ground, and are consistent with measured values of the Total Electron Content for equatorial regions, reported by [*Ezquer et al*, 1994]. These values may, however, overestimate the electron content, since the 'equivalent slab thickness' of the ionosphere is likely to be less than the satellite altitude, h_s. Thus the values of Ω given in the table should be regarded as upper limits for the actual Ω values.

Table 1. Ranges of critical frequency, electron density, integrated electron content, and the Faraday rotation angle for a radar in a 568 km, polar orbit, with a 38.5 degree look angle over the tropical region ($\pm 15^{o}$ from the equator). Faraday rotation angles are given for C-Band (6 cm wavelength), L-Band (24 cm wavelength), and P-Band (68 cm wavelength).

	Midnight		Midday	
	Minimum	Maximum	Minimum	Maximum
$f_c(MC/S)$	5	9	11	12
N (electrons/m^3)	0.31×10^{12}	1.004×10^{12}	1.5×10^{12}	2.79×10^{12}
I_s (electrons/m^2)	1.76×10^{17}	5.7×10^{17}	8.52×10^{17}	1.59×10^{18}
Ω_C (degrees)	0.3^o	0.9^o	1.4^o	2.6^o
Ω_L (degrees)	4.6^o	14.8^o	22.05^o	41.0^o
Ω_P (degrees)	36.61^o	118.6^o	177.0^o	329.5^o

As a result of propagation through the ionosphere, Faraday rotation affects the SAR system both in azimuth and range direction in a complex fashion. In the range direction, the effect can be compensated during the range compression because the antenna is fixed with respect to the scatterers in a given range pulse. In the azimuth direction, the antenna moves relative to the scatterers and the Faraday rotation factors are convolved with the scattered wave from the scene [*Rosen*, 1992; *Gail*, 1998]. In what follows, we will consider only the net Faraday rotation in the final image product, i.e. the result of both azimuth and range compression.

Modeling The Effect On Backscatter Signatures

By assuming that there is no variation of Faraday rotation across the SAR antenna beam, linearly polarized waves transmitted and received by the SAR system can experience two incidences of Faraday rotation, one downgoing and one upgoing. The sense of Faraday rotation in each direction is the same relative to the Earth's magnetic field and is independent of the propagation direction. For a general case, assume the transmitted electric field, $\mathbf{E}_t$ can be represented in terms of horizontal and vertical field components. After one way transmission through the ionosphere, the field incident, **B**, on the Earth's surface is rotated by the Faraday rotation matrix $\mathbf{R}_F$ such that $\mathbf{E}_i = \mathbf{R}_F \mathbf{E}_t$. The scattered field from the target (distributed target in case of land surface) undergoes another rotation along the receive propagation path before reaching the antenna. Therefore, the elements of the scattering matrix, **S**, of the target are modified as a result of the round-trip Faraday rotation angle. For a SAR system measuring linear horizontal (H) and vertical (V) polarizations in the antenna coordinate system, the measured scattering matrix, **M**, can be written, [after *Gail*, 1993 and *Rosen*, 1992], as:

$$\mathbf{M} = Ae^{j\phi}\,\mathbf{R}^T\mathbf{R}_F\mathbf{S}\mathbf{R}_F\mathbf{T} + \mathbf{N} \qquad (4)$$

where **S** is the scattering matrix, $\mathbf{R}_F$ represents the one-way Faraday rotation matrix, **R** is the receive distortion matrix (of the radar system) and **T** is the transmit distortion matrix (of the radar system). Both **R** and **T** include cross-talk and channel amplitude and phase imbalance terms. The (real) factor A represents the overall gain of the radar system, and the complex factor $e^{j\phi}$ represents the round-trip phase delay and system-dependent phase effects on the signal. The matrix **N** represents additive noise terms present in each measurement due to Earth radiation, thermal fluctuations in the receiver, and digitization noise.

Calibration techniques have been described [e.g. in *Freeman*, 1992] which can successfully estimate and correct for the system-dependent terms A, **R** and **T**. Assume for the moment that the system under consideration is either so well-calibrated that A, **R** and **T** can be ignored or sufficiently stable that estimates for A, **R** and **T** obtained when no Faraday rotation is present can be applied to measurements obtained when Faraday rotation is present. The complex term $e^{j\phi}$ is usually ignored except in the case of interferometric data analysis. If the Signal-to-Noise ratio is high enough, the additive noise terms in **N** can also be ignored, for now. Making these assumptions, (4) becomes simply:

$$\mathbf{M} = \mathbf{R_F S R_F} \tag{5}$$

Equation (5) can be expanded to show the nature of the problem when Faraday rotation alone is the measurement error source:

$$\begin{bmatrix} M_{hh} & M_{vh} \\ M_{hv} & M_{vv} \end{bmatrix} = \begin{bmatrix} \cos\Omega & \sin\Omega \\ -\sin\Omega & \cos\Omega \end{bmatrix} \begin{bmatrix} S_{hh} & S_{vh} \\ S_{hv} & S_{vv} \end{bmatrix} \begin{bmatrix} \cos\Omega & \sin\Omega \\ -\sin\Omega & \cos\Omega \end{bmatrix} \tag{6}$$

which can be written:

$$M_{hh} = S_{hh}\cos^2\Omega - S_{vv}\sin^2\Omega + \left(S_{hv} - S_{vh}\right)\sin\Omega\cos\Omega \tag{7a}$$

$$M_{vh} = S_{vh}\cos^2\Omega + S_{hv}\sin^2\Omega + \left(S_{hh} + S_{vv}\right)\sin\Omega\cos\Omega \tag{7b}$$

$$M_{hv} = S_{hv}\cos^2\Omega + S_{vh}\sin^2\Omega - \left(S_{hh} + S_{vv}\right)\sin\Omega\cos\Omega \tag{7c}$$

$$M_{vv} = S_{vv}\cos^2\Omega - S_{hh}\sin^2\Omega + \left(S_{hv} - S_{vh}\right)\sin\Omega\cos\Omega \tag{7d}$$

Invoking backscatter reciprocity, i.e. $S_{hv} = S_{vh}$,

$$M_{hh} = S_{hh}\cos^2\Omega - S_{vv}\sin^2\Omega \tag{8a}$$

$$M_{vh} = S_{hv} + \left(S_{hh} + S_{vv}\right)\sin\Omega\cos\Omega \tag{8b}$$

$$M_{hv} = S_{hv} - \left(S_{hh} + S_{vv}\right)\sin\Omega\cos\Omega \tag{8c}$$

$$M_{vv} = S_{vv}\cos^2\Omega - S_{hh}\sin^2\Omega \tag{8d}$$

Note that for cross-pol measurements, the presence of non-zero Faraday rotation means that they will not necessarily be reciprocal, i.e. $M_{hv} \neq M_{vh}$.

HH polarization measurements only

Several spaceborne SARs have been flown which measure L-Band HH polarization backscatter only, i.e. Seasat SAR, SIR-A, SIR-B and JERS-1. The expected value of the radar cross section measured by these radars in the presence of Faraday rotation is:

$$\left\langle M_{hh} M_{hh}^* \right\rangle = S_{hh} S_{hh}^* \cos^4\Omega - 2\mathrm{Re}\left(S_{hh} S_{vv}^*\right)\sin^2\Omega\cos^2\Omega + S_{vv} S_{vv}^* \sin^4\Omega \tag{9}$$

We have also modeled the effect of Faraday rotation on Repeat-pass Interferometry measurements made by HH polarization only spaceborne radars. This is done by correlating a 'nominal' measurement of S_{hh} with zero rotation with a subsequent rotated measurement as given in (8), to give:

$$\left\langle M_{hh_1} M^*_{hh_2} \right\rangle = S_{hh_1} S^*_{hh_2} \cos^2\Omega - S_{hh_1} S^*_{vv_2} \sin^2\Omega \tag{10}$$

Assuming no change in the backscatter, i.e. that there is no temporal decorrelation, we can assess the decorrelation introduced by Faraday rotation alone:

$$\left\langle M_{hh_1} M^*_{hh_2} \right\rangle = S_{hh} S^*_{hh} \cos^2\Omega - S_{hh} S^*_{vv} \sin^2\Omega \tag{11}$$

As a normalized correlation coefficient, this can be expressed as:

$$\rho_{\text{Faraday}} = \frac{\left| \left\langle M_{hh_1} M^*_{hh_2} \right\rangle \right|}{\sqrt{\left\langle M_{hh_1} M^*_{hh_1} \right\rangle \left\langle M_{hh_2} M^*_{hh_2} \right\rangle}}$$

or

$$\rho_{\text{Faraday}} = \frac{\left| \left(S_{hh} S^*_{hh} \cos^2\Omega - S_{hh} S^*_{vv} \sin^2\Omega \right) \right|}{\sqrt{\left(S_{hh} S^*_{hh} \right) \left(S_{hh} S^*_{hh} \cos^4\Omega - 2\text{Re}\left(S_{hh} S^*_{vv} \right) \sin^2\Omega \cos^2\Omega + S_{vv} S^*_{vv} \sin^4\Omega \right)}} \tag{12}$$

which does not include temporal decorrelation or noise decorrelation.

Dual-polarized (HH and HV) measurements

The SIR-C radar instrument had one mode in which only HH and HV measurements were made at a given frequency. This allowed for wider swaths to be illuminated than fully polarimetric modes because of the lower data rates. This type of data collection has also been proposed for other planned spaceborne SARs such as NASA's LightSAR and the Japanese Space Agency's PALSAR. Forming cross-products between

the appropriate scattering matrix terms in (8), we obtain, for dual-polarized measurements in the presence of Faraday rotation:

$$\left\langle M_{hh}M_{hh}^{*}\right\rangle = S_{hh}S_{hh}^{*}\cos^{4}\Omega - 2\mathrm{Re}\left\{S_{hh}S_{vv}^{*}\right\}\sin^{2}\Omega\cos^{2}\Omega + S_{vv}S_{vv}^{*}\sin^{4}\Omega \tag{13a}$$

$$\left\langle M_{hv}M_{hv}^{*}\right\rangle = S_{hv}S_{hv}^{*} + \sin^{2}\Omega\cos^{2}\Omega\left(S_{hh}S_{hh}^{*} + S_{vv}S_{vv}^{*} + 2\mathrm{Re}\left\{S_{hh}S_{vv}^{*}\right\}\right) \tag{13b}$$

$$\left\langle M_{hh}M_{hv}^{*}\right\rangle = \sin\Omega\cos\Omega\left(-S_{hh}S_{hh}^{*}\cos^{2}\Omega - S_{hh}S_{vv}^{*}\cos^{2}\Omega - S_{vv}S_{hh}^{*}\sin^{2}\Omega + S_{vv}S_{vv}^{*}\sin^{2}\Omega\right) \tag{13c}$$

where we have assumed that reflection symmetry holds, as is the case for most natural targets, with the consequence that:

$$\left\langle S_{hh}S_{hv}^{*}\right\rangle = \left\langle S_{hv}S_{vv}^{*}\right\rangle = 0 \tag{14}$$

Quad-polarized measurements

SIR-C also made fully polarimetric or quad-pol backscatter measurements. Such measurements are also planned for the LightSAR L-Band radar system. During the calibration of SIR-C polarimetric data, a symmetrization operation was performed. In the process of symmetrization, the cross-product between the two cross-pol measurements is used to assess any amplitude or phase imbalance between these two channels. This cross-product, from (8b) and (8c), would be:

$$\left\langle M_{hv}M_{vh}^{*}\right\rangle = S_{hv}S_{hv}^{*} - \left(S_{hh}S_{hh}^{*} + S_{vv}S_{vv}^{*} + 2\mathrm{Re}\left\{S_{vv}S_{vv}^{*}\right\}\right)\sin^{2}\Omega\cos^{2}\Omega \tag{15}$$

If the phase or amplitude of this cross-product exceeded certain thresholds when compared with default system values, the default values were used in symmetrization. The net effect would be to add the HV and VH measurements after correction for all system-dependent phase and amplitude imbalances, i.e. the composite 'symmetrized' HV measurement would be obtained from:

$$M_{hv}' = 0.5\left(M_{hv} + M_{vh}\right) \equiv S_{hv} \tag{16}$$

Thus for properly 'symmetrized' cross-pol data, the Faraday rotation should have no effect on the measured backscatter value. Forming cross-products from (8a), (8d) and (16), and assuming that like- and cross-polarized backscatter measurements are uncorrelated as in (14), we obtain:

$$\begin{aligned}
\left\langle M_{hh}M_{hh}^{*}\right\rangle &= S_{hh}S_{hh}^{*}\cos^4\Omega - 2\mathrm{Re}\left\{S_{hh}S_{vv}^{*}\right\}\sin^2\Omega\cos^2\Omega + S_{vv}S_{vv}^{*}\sin^4\Omega \\
\left\langle M_{hv}M_{hv}^{*}\right\rangle &= S_{hv}S_{hv}^{*} \\
\left\langle M_{vv}M_{vv}^{*}\right\rangle &= S_{hh}S_{hh}^{*}\sin^4\Omega - 2\mathrm{Re}\left\{S_{hh}S_{vv}^{*}\right\}\sin^2\Omega\cos^2\Omega + S_{vv}S_{vv}^{*}\cos^4\Omega \\
\left\langle M_{hh}M_{vv}^{*}\right\rangle &= S_{hh}S_{vv}^{*}\cos^4\Omega - \left(S_{hh}S_{hh}^{*} + S_{vv}S_{vv}^{*}\right)\sin^2\Omega\cos^2\Omega + S_{vv}S_{hh}^{*}\sin^4\Omega \\
\left\langle M_{hh}M_{hv}^{*}\right\rangle &= 0 \\
\left\langle M_{hv}M_{vv}^{*}\right\rangle &= 0
\end{aligned} \tag{17}$$

where again only the like-pol terms are affected by the Faraday rotation. A corollary of this is that, if the default 'symmetrization' is not successful, the effects would quickly be evident as non-zero $M_{hh}M_{hv}^{*}$ and $M_{hv}M_{vv}^{*}$ terms.

Model Results

To determine what will happen to backscatter measurements affected by Faraday rotation, it is clear that the full scattering matrix should be known. The polarimetric backscatter measurements in Tables 2 and 3 were extracted from L-Band and P-Band polarimetric SAR data collected by the NASA/JPL AIRSAR system over a tropical rain forest in Belize during 1991 and over a site in Raco, Northern Michigan in June 1991. For this data Faraday rotation is definitely not a problem. They are presented here as typical of scattering from natural terrain. The behavior of the scattering from bare soil is representative of scattering observed from similar fields around the world, for example. The scattering behavior for pasture is typical of grassland areas; the upland forest signature is representative of broadleaf forests in other areas; the swamp forest is an example of a forest with a high degree of double-bounce as well as canopy scatter, because of flooding beneath the canopy; and the plantation and conifer areas are different examples of forests which exhibit a high degree of double-bounce as well as canopy scatter because of a relatively sparse canopy, which is more transparent to longer wavelength radar waves.

L-Band	HH σ^o (dB)	HV σ^o (dB)	VV σ^o (dB)	HH-VV Phase (deg.)	HH-VV Correlation
Bare Soil	-16.5	-26.9	-14.7	-23.7	0.75
Pasture	-13.3	-25	-11.8	-18.6	0.75
Upland Forest	-9.2	-14.3	-9.4	7.9	0.25
Swamp Forest	-6.9	-14.5	-7.3	165.4	0.06
Plantation	-8	-15.7	-9.7	52.1	0.12
Conifers	-6.2	-13.1	-8.9	36.9	0.21

Table 2: L-Band backscatter measurements from NASA/JPL AIRSAR data for a variety of land cover types

P-Band	HH σ^o (dB)	HV σ^o (dB)	VV σ^o (dB)	HH-VV Phase (deg.)	HH-VV Correlation
Bare Soil	-25.1	-34.6	-19.7	-8.8	0.75
Pasture	-20.3	-31.8	-18.3	-12.5	0.53
Upland Forest	-11.5	-17.9	-11.9	51.1	0.14
Swamp Forest	-13.8	-22.2	-13.2	149.5	0.10
Plantation	-9.2	-18	-10.5	137.3	0.40
Conifers	-5.5	-14.5	-9.8	78.5	0.29

Table 3: P-Band backscatter measurements from NASA/JPL AIRSAR data for a variety of land cover types

Although the absolute value of the P-Band backscatter in dB is typically lower than that for L-Band, the polarimetric behavior tends to be broadly similar. For example, bare soil has a fairly low HV backscatter at both frequencies, a high correlation between the like-pol measurements, a fairly small phase difference between the like-pol measurements, and the VV backscatter is higher than the HH. This is typical of scattering from slightly rough surfaces, as discussed in [*Freeman and Durden*, 1992], which is represented by:

Small Perturbation Model

$$\begin{aligned}
&\langle S_{vv} S_{vv}^* \rangle = b^2 \langle S_{hh} S_{hh}^* \rangle; \\
&\langle S_{hh} S_{vv}^* \rangle = b \langle S_{hh} S_{hh}^* \rangle; \; b \text{ real}, b > 1 \\
&\langle S_{hv} S_{hv}^* \rangle = 0; \\
&\langle S_{hh} S_{hv}^* \rangle = \langle S_{hv} S_{vv}^* \rangle = 0
\end{aligned} \tag{18}$$

The upland forest backscatter is typical of scattering from azimuthally symmetric scatterers [*Nghiem et al*, 1992], which have the following general properties:

Azimuthal Symmetry

$$\begin{aligned}
&\langle S_{hh} S_{hh}^* \rangle = \langle S_{vv} S_{vv}^* \rangle; \\
&\langle S_{hh} S_{vv}^* \rangle = \varepsilon \langle S_{hh} S_{hh}^* \rangle, \; \varepsilon \text{ real}; \\
&\langle S_{hv} S_{hv}^* \rangle = (1 - 2\varepsilon) \langle S_{hh} S_{hh}^* \rangle; \\
&\langle S_{hh} S_{hv}^* \rangle = \langle S_{hv} S_{vv}^* \rangle = 0
\end{aligned} \tag{19}$$

For the forest types with significant double-bounce scatter (i.e. the plantation, swamp forest and conifers), the following model has been used for the double-bounce contribution:

Double-bounce

$$\begin{aligned}
&\langle S_{vv} S_{vv}^* \rangle = |\alpha|^2 \langle S_{hh} S_{hh}^* \rangle; \\
&\langle S_{hh} S_{vv}^* \rangle = \alpha \langle S_{hh} S_{hh}^* \rangle, \; \alpha \text{ complex}; \\
&\langle S_{hv} S_{hv}^* \rangle = 0 \\
&[\text{Typically } |\alpha| < 1, \arg(\alpha) \approx \pm\pi]
\end{aligned} \tag{20}$$

Since canopy scatter and the ground-trunk term are usually present together in the same return, double-bounce and azimuthally symmetric (i.e. canopy) scattering need to be combined in some proportion f_d:f_v, as in [*Freeman and Durden*, 1992], to give:

Rotational Symmetry + Double-bounce

$$\begin{aligned}
\langle S_{hh} S_{hh}^* \rangle &= f_v + f_d; \\
\langle S_{vv} S_{vv}^* \rangle &= f_v + |\alpha|^2 f_d \\
\langle S_{hh} S_{vv}^* \rangle &= \varepsilon f_v + \alpha f_d; \\
\langle S_{hv} S_{hv}^* \rangle &= (1 - 2\varepsilon) f_v; \\
\langle S_{hh} S_{hv}^* \rangle &= \langle S_{hv} S_{vv}^* \rangle = 0
\end{aligned} \tag{21}$$

For $f_d \approx f_v$, the expected behavior of the combined scattering represented by eq. (21) has the following properties:

$$\begin{aligned}
&\langle S_{hh} S_{hh}^* \rangle \geq \langle S_{vv} S_{vv}^* \rangle; \\
&\rho_{hhvv} < \varepsilon ; \\
&\mathrm{Re} \langle S_{hh} S_{vv}^* \rangle < 0
\end{aligned} \tag{22}$$

The chief difference between L- and P-Band measurements subject to Faraday rotation is evident from Table 1, i.e. the Faraday rotation angle Ω for P-Band should be much larger. In what follows the results of the model simulation will be presented for only one frequency at a time, unless the results are significantly different in behavior. The effects of Faraday rotation will be plotted for various backscatter measurements as a function of the Faraday rotation angle Ω, over the range 0 to 180 degrees. It is not necessary to plot over a larger range of Ω since it is quite easy to show that:

$$\mathbf{M}(\Omega) = \mathbf{R}_F(\Omega)\, \mathbf{S}\, \mathbf{R}_F(\Omega) = \mathbf{M}(\Omega \pm \pi) \tag{23}$$

HH polarization measurements only

The L-Band polarimetric backscatter measurements given in Table 2 were inserted into equation (7) in order to estimate the effect on measurements made by a radar capable only of transmitting and receiving H-polarized waves. The results are summarized in

Figure 1. From the figure, it is clear that the maximum Faraday rotation angle of 40 degrees at L-Band will lead to a significant drop in the measured backscatter level for all scatterer types. Results for P-Band show similar behavior, as can be seen from Figure 2.

Referring to Table 1, the maximum Faraday rotation angle expected for an L-Band spaceborne radar system is ~41 degrees. There is some variation in the HH backscatter measurement due to the different polarization signatures over the full range of Faraday rotation angles, but no very significant differences between the different scattering types over the range 0 to 40 degrees. Thus at L-Band we would expect the most visible effect of Faraday rotation to be a general lowering in the measured backscatter, by as much as 3 or 4 dB, comparing results at 0 degree rotation to those at about 40 degrees. Comparing data-takes with Faraday rotation and without Faraday rotation over similar areas, the most noticeable effect would be a drop in overall Signal-to-Noise ratio in the former case (assuming that the noise level is the same in each case).

The general behavior shown in Figures 1 and 2 can readily be reproduced by inserting the modeled polarization signatures in (18), (19) and (21) into eq. (9). Thus for slightly rough surfaces, there is a zero point in the predicted 'HH' measurement for $\Omega = 45$ degrees, and at $\Omega = 90$ degrees, the 'HH' measurement is equal to the VV backscatter value, which is larger than the HH backscatter value. For azimuthally symmetric scatterers, the predicted 'HH' measurement for $\Omega = 45$ degrees is the same as the HV backscatter value, and again at $\Omega = 90$ degrees, the 'HH' measurement is equal to the VV backscatter value (though both HH and VV values are the same in this case). For mixed azimuthally symmetric and double-bounce scatterers, the predicted 'HH' measurement for $\Omega = 45$ degrees is significantly greater than the HV backscatter value, and again at $\Omega = 90$ degrees, the 'HH' measurement is equal to the VV backscatter value, which is typically less than or equal to the HH backscatter value.

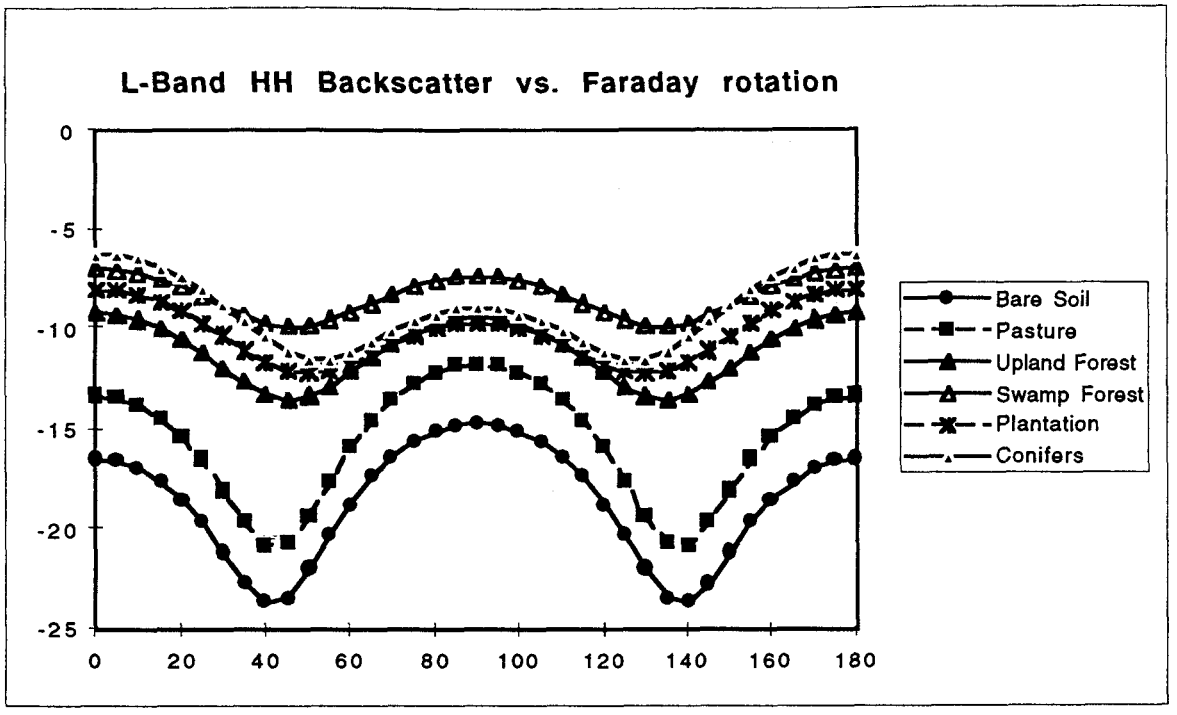

Figure 1: Predicted backscatter values as measured by an L-Band H-transmit, H-receive radar for different backscatter types as a function of Faraday rotation angle, Ω.

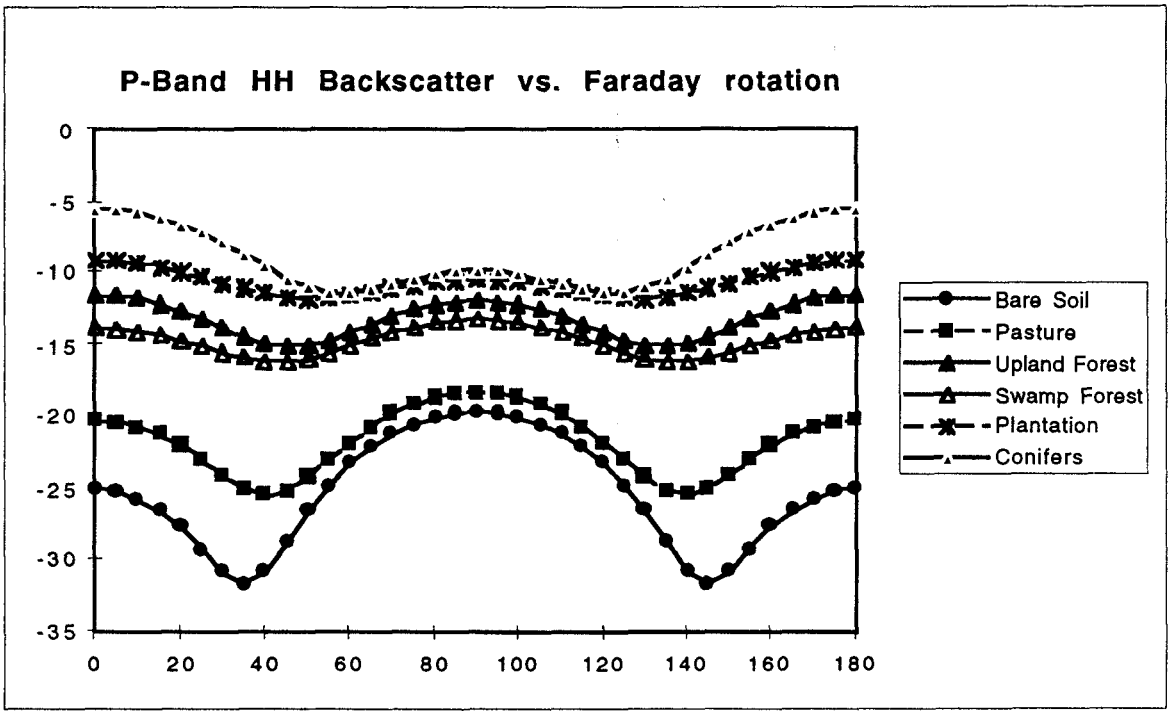

Figure 2: Predicted backscatter values as measured by a P-Band H-transmit, H-receive radar for different backscatter types as a function of Faraday rotation angle, Ω.

The effect of Faraday rotation on Repeat-pass Interferometry measurements made by a spaceborne SAR has also been modeled using equation (12). A typical noise floor level of -30 dB was included in the denominator of the calculated correlation coefficients: thus the correlation is never identical to unity, even when the ionosphere has no effect (case $\Omega = 0$). Temporal decorrelation due to changes in physical characteristics have not been considered for any of the backscatter types. It can be seen from the figure that the correlation coefficients are not much affected by Faraday rotation up to $\Omega = 30$ degrees, but then drop off markedly for larger angles. For $\Omega = 90$ degrees, the correlation coefficient is actually the same as the HH-VV correlation coefficient, as can be seen by comparing the values in Figure 3 with the appropriate column in Table 2. Thus the effect of Faraday rotation may be noticeable in repeat-pass interferometry data as a general decrease in the temporal correlation coefficients, and if Ω is close to 90 degrees (or 270 degrees), high values for the correlation coefficient may be observed in non-forested areas, and low correlation coefficient values in forested areas.

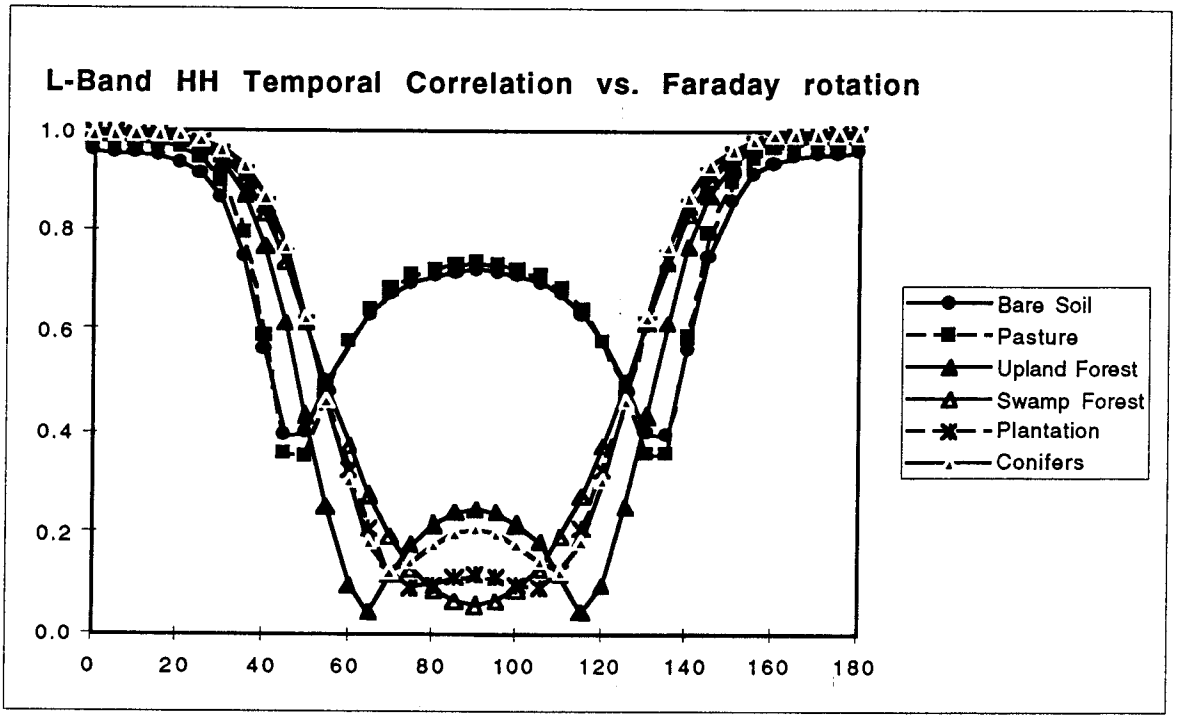

Figure 3: Modeled correlation coefficients for nominally HH polarization repeat-pass measurements of the different backscatter types from Table 2, including decorrelation due to system noise at -30 dB and Faraday rotation through angle Ω.

Dual-polarized (HH and HV) measurements

If only nominal HH and HV measurements are available, it is interesting to look at the behavior of the measured 'HV' backscatter values and the measured 'HH-HV' correlation coefficient with Faraday rotation angle, as estimated from equation (13). These are shown in Figures 4 and 5. The correlation coefficients were estimated using a noise floor of -30 dB. The cyclic behavior visible in Figure 4 stems from the $(\sin 2\Omega)^2$ dependence of the like-pol contributions to the 'HV' backscatter measurement in equation (13b), which are maximum for $\Omega = 45$ degrees. Comparing Figures 4 and 1, we see that it is possible to have the nominal HV backscatter measurement be larger than the nominal HH backscatter measurement, e.g. for $\Omega = 45$ degrees. This situation almost never occurs due to scattering in nature, so should be simple to detect in the data.

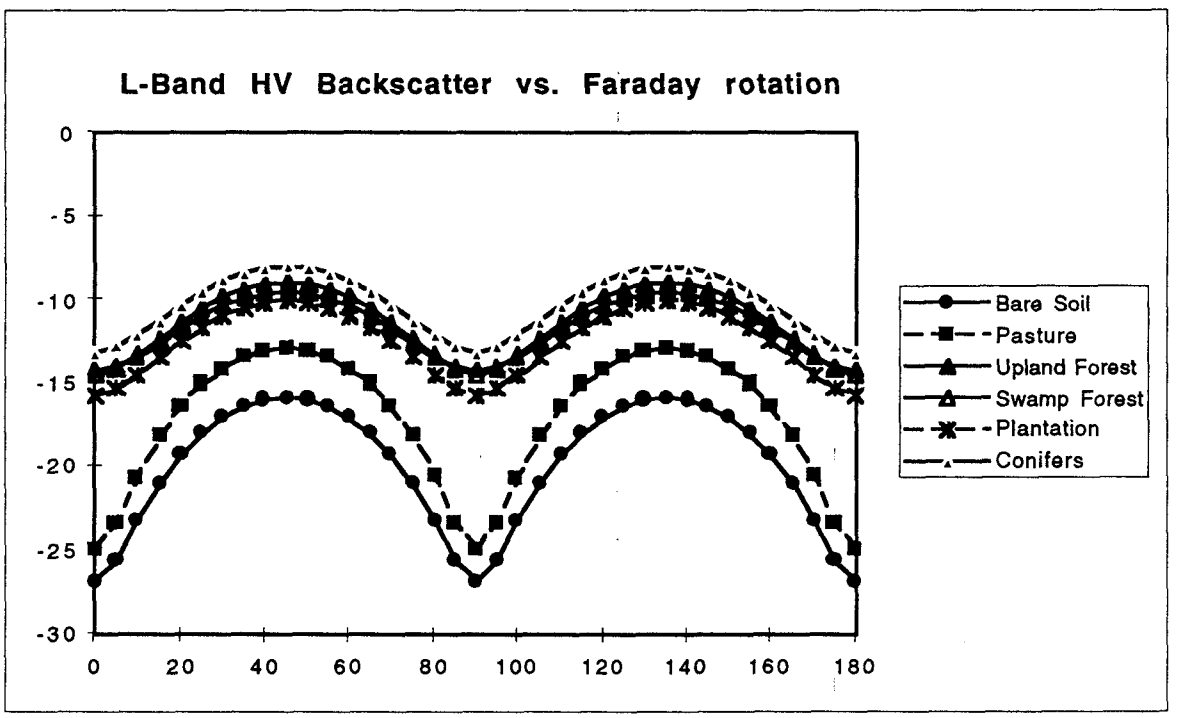

Figure 4: Modeled L-Band backscatter for a nominally HV polarized measurement (dual-polarized data) versus Faraday rotation for the different backscatter types

The definite null visible in the HH-HV correlation values plotted in Figure 5 at $\Omega = 90$ degrees stems from the $\sin 2\Omega$ dependence of the 'HH-HV' correlation measurement in equation (13c). There is also a less pronounced null at around $\Omega = 45$ degrees. The figure indicates that a small Faraday rotation angle of around 20 degrees should be detectable as an increase in the measured 'HH-HV' correlation coefficient, which is usually close to zero

for most natural scatterers. Except for Ω = 0, 90 or 180 degrees, the HH-HV correlation coefficient will also exhibit significant differences depending on the type of scatterer, especially between forested/non-forested areas.

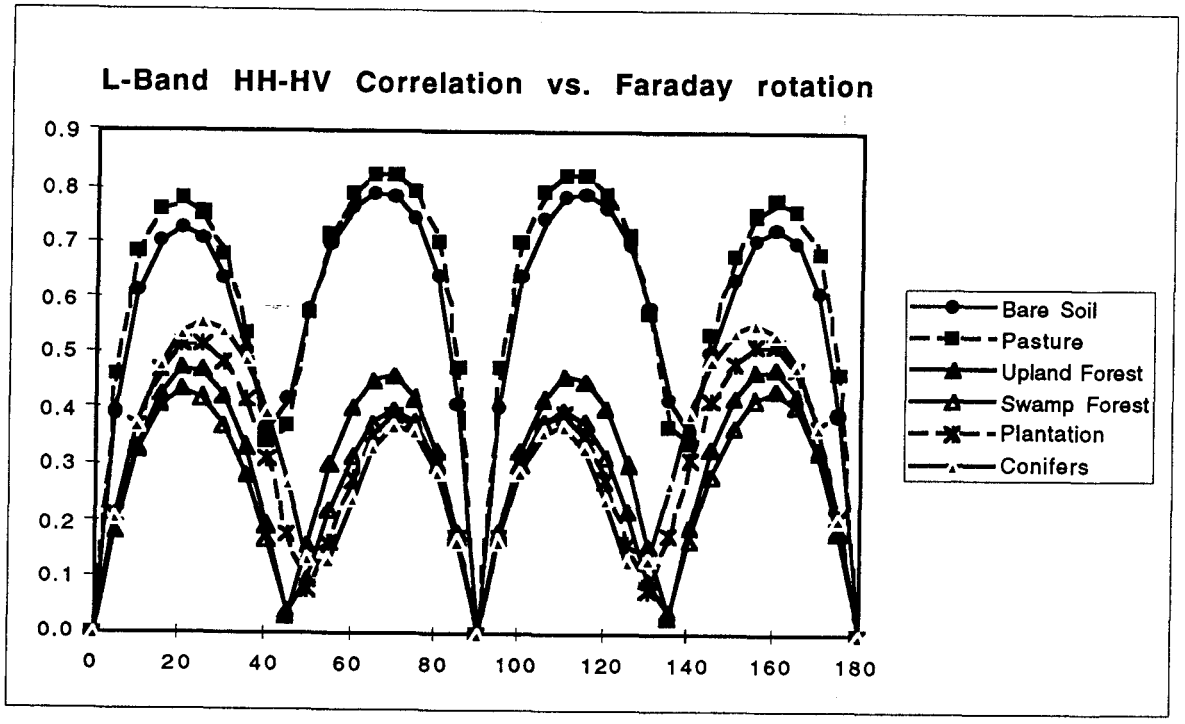

Figure 5: Modeled L-Band 'HH-HV' correlation coefficient measurement (dual-polarized data) versus Faraday rotation for the different backscatter types from Table 2.

Quad-polarized measurements

Returning to equation (15), we can plot the transition of the phase of the nominal HVVH* phase difference as a function of Faraday rotation angle, as in Figure 6. From the Figure, we see that for small values of Ω, the phase of the measured HVVH* is zero for all scatterers. This quickly flips to 180 degrees (i.e. HVVH* becomes negative) as Ω increases, then flips to zero again close to 90 degrees and then cycles once more as Ω goes from 90 to 180 degrees. Thus a relatively small Faraday rotation angle may be detectable as a 180 degree phase change in the measured HVVH* term. This is particularly relevant for SIR-C polarimetric L-Band data, for which HVVH* was routinely monitored during data processing.

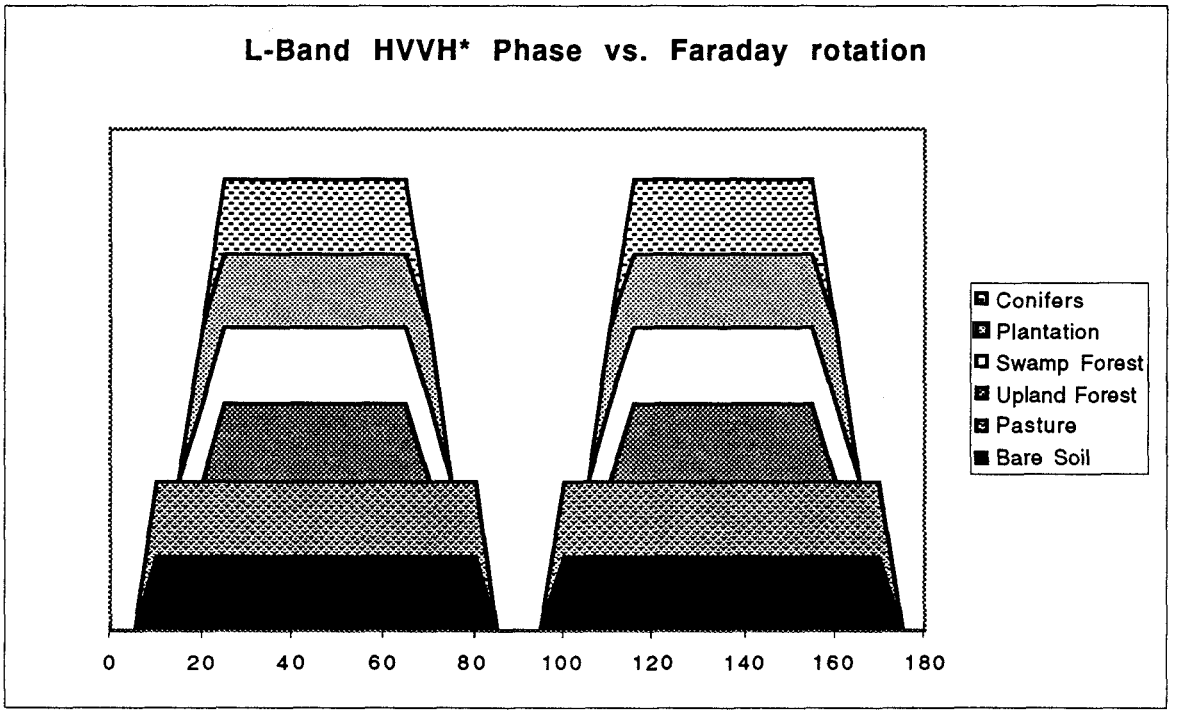

Figure 6: Modeled L-Band 'HVVH*' phase transitions versus Faraday rotation for the different backscatter types from Table 2.

The behavior of the measured 'HHVV*' phase difference versus Faraday rotation was modeled using the appropriate term in equation (17). The results are a little more difficult to interpret, but are clearly backscatter-dependent, as can be seen from Figure 7. For the swamp forest, the measured 'HHVV*' phase difference hardly changes at all, while for the bare soil, pasture and upland forest, the measured 'HHVV*' phase difference cycles through 360 degrees over the range of Ω.

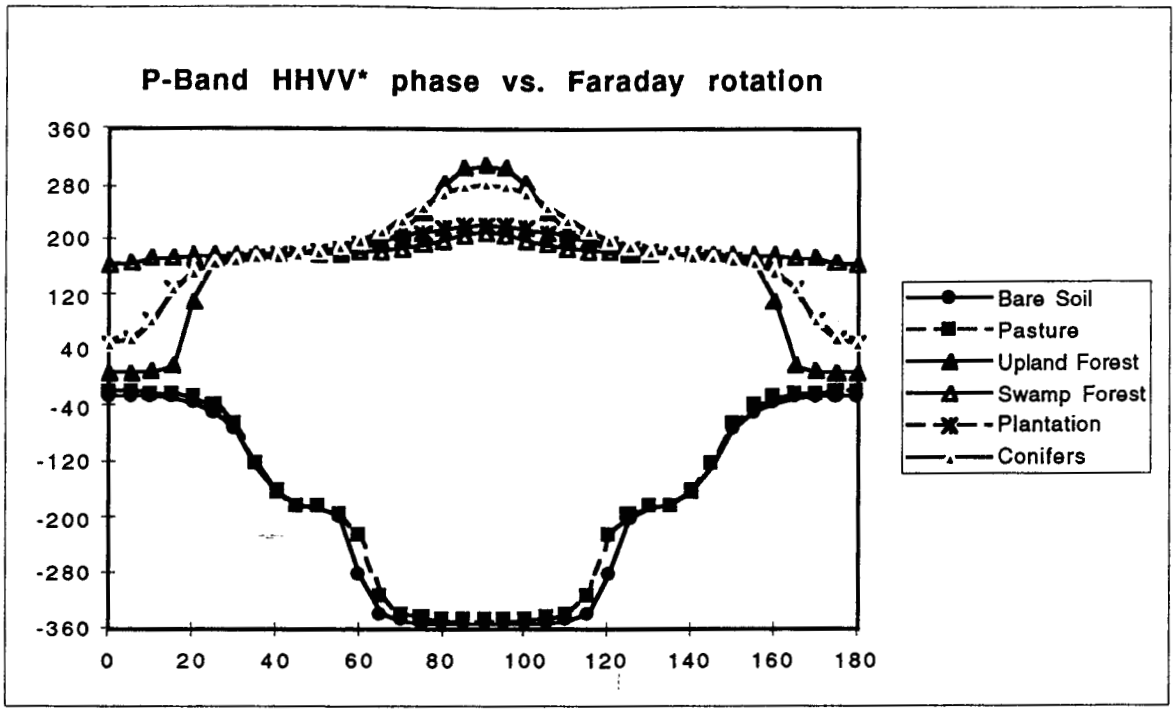

Figure 7: Modeled P-Band 'HHVV*' phase measurements versus Faraday rotation for the different backscatter types from Table 3.

The behavior of the measured 'HHVV*' correlation coefficient versus Faraday rotation was also modeled by forming a correlation coefficient from the appropriate terms in equation (17). The results are shown in Figure 8. The plots show a peak in the correlation at $\Omega = 45$ degrees. Returning to equation (8a) and (8d) we can see that the 'HH' and 'VV' backscatter measurements will be identical for $\Omega = 45$ and 135 degrees, hence the high value for the correlation coefficient.

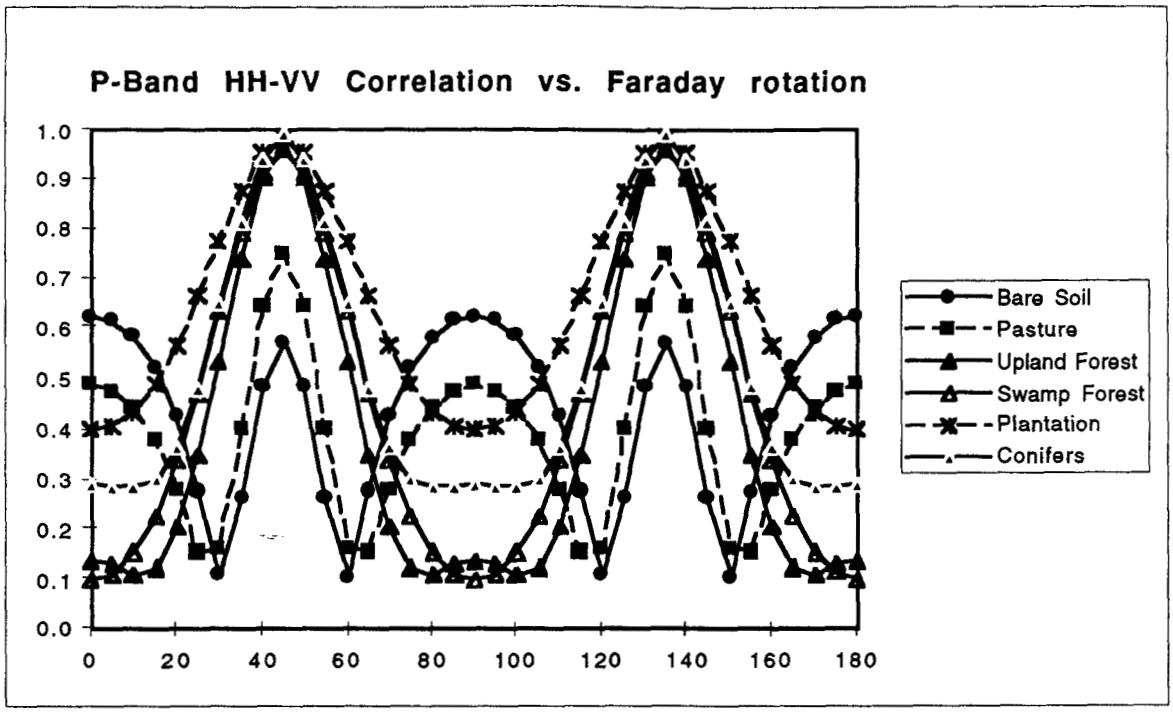

Figure 8: Modeled P-Band 'HHVV*' correlation measurements versus Faraday rotation for the different backscatter types from Table 3.

Finally, the model results for a nominal 'VV' backscatter measurement versus Faraday rotation angle are shown in Figure 9. The results are similar to those in Figure 1 for 'HH' measurements. Perhaps the most notable feature seen in comparing the plots shown in Figures 9 and 1 is the way that the HH and VV measurements 'trade places' for $\Omega = 90$ degrees.

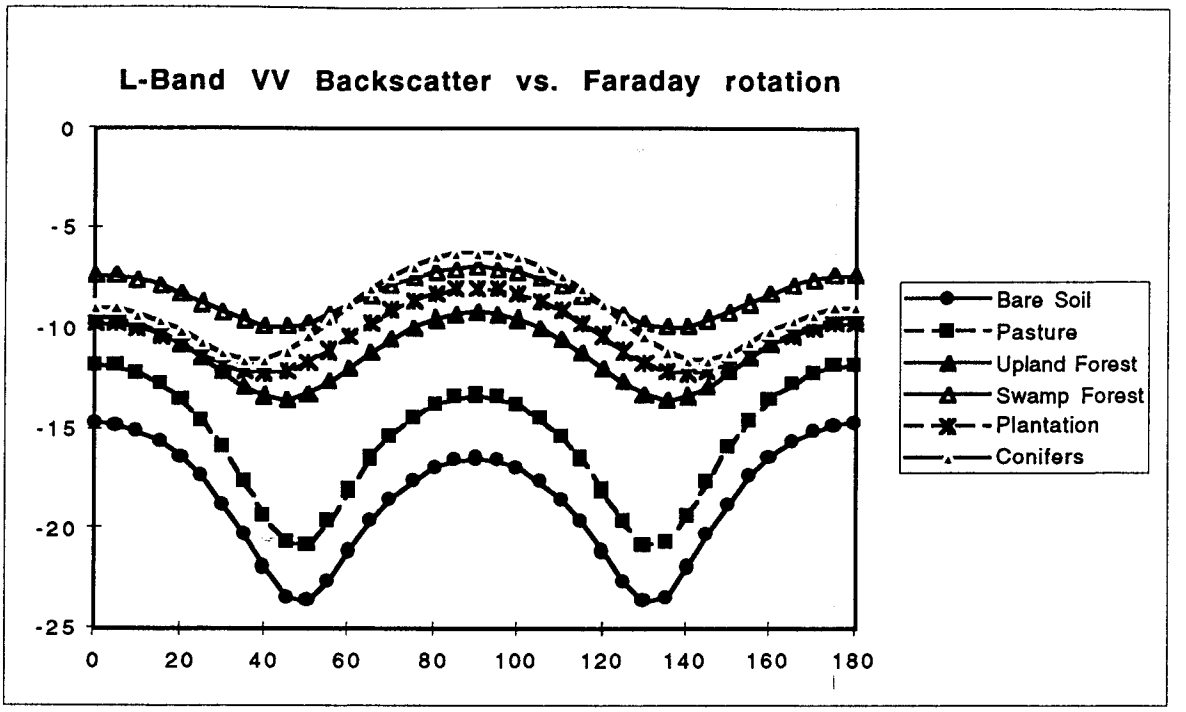

Figure 9: Modeled L-Band backscatter for a nominally VV polarized measurement versus Faraday rotation for the different backscatter types in Table 2

Estimation and Correction of Faraday Rotation

Previous sections have modeled the effects of Faraday rotation on spaceborne radar backscatter measurements and discussed whether these effects might be identified from measured data. This section addresses the problem of estimating the Faraday rotation Ω, and correcting measured data.

HH polarization measurements only

From equation (7), which has four unknowns, it is clear that there is no possible way to unambiguously estimate Ω from single-pol measurements. Even if Ω were known by other means, it is not possible to correct the HH backscatter measurements without knowledge of the VV backscatter.

Dual-polarized (HH and HV) measurements

Referring to the HH and HV backscatter measurements in (6a) and (6b) we have two equations with 4 unknowns. Forming cross-products as in (11) this becomes 3 equations in 5 unknowns (assuming that like- and cross-polarized scattering matrix terms are uncorrelated). It is clear that, to estimate Ω from dual-polarized measurements, some assumptions about the polarimetric behavior of the scatterers are necessary. Two possibilities are the models for scattering from slightly rough surfaces and rotationally symmetric scatterers given in equations (15) and (16). Analysis of using a slightly rough surface model reveals that it does not provide enough information to estimate Ω, since one of the equations in (11) becomes redundant. When inserted into (11), the rotationally symmetric model in (16) does provide enough information to estimate Ω, but only modulo $\pi/2$, which is not sufficient to correct the dual-polarized measurements. Thus we conclude that it may be possible to detect the presence of Faraday rotation in dual-polarized data, but only to within $\pi/2$. If the maximum values in Table 1 are correct, this would mean that it is possible to unambiguously estimate the Faraday rotation in L-Band but not P-Band dual-polarized data. In either case, correction for the Faraday rotation angle is not possible, since again one of the scattering terms (i.e. the VV term) is unknown.

Quad-polarized measurements

For the case where Faraday rotation is the only significant error source, and fully polarimetric (linear polarized) measurements are available, it is straightforward to start from equation (8) and estimate the Faraday rotation angle, Ω, via:

$$\Omega = \frac{1}{2}\tan^{-1}\left[\frac{\left(M_{vh} - M_{hv}\right)}{\left(M_{hh} + M_{vv}\right)}\right] \tag{24}$$

for any type of scatterer (other, additional calibration error sources are considered in the Appendix.) Since speckle and additive noise may be present in the backscatter signatures, a more robust approach to estimate Ω may use averaged second-order statistics, by first calculating:

$$Z_{hv} = 0.5\left(M_{vh} - M_{hv}\right) \tag{25}$$

then estimating Ω from:

$$\Omega = \frac{1}{2}\tan^{-1}\sqrt{\frac{\left\langle Z_{hv}Z_{hv}^{*}\right\rangle}{\left(\left\langle M_{hh}M_{hh}^{*}\right\rangle + \left\langle M_{vv}M_{vv}^{*}\right\rangle + 2\,\mathrm{Re}\left\{\left\langle M_{hh}M_{vv}^{*}\right\rangle\right\}\right)}} \tag{26}$$

(The HH and VV backscatter measurements in (26) may be corrected for additive noise if the noise powers in each measurement channel are sufficiently well-known.)

To arrive at equations (24) and (26) for Ω, the only assumptions necessary are that backscatter reciprocity holds, and that Faraday rotation is the only source of calibration error. These equations are also valid even when the cross-pol backscatter contribution goes to zero (e.g. for surface scattering only, as in eq. (18)). Thus Ω can be estimated from any monostatic scattering signature, or *for all scatterers within a strip map SAR image obtained over land or ocean.*

To correct for a Faraday rotation of Ω, the following matrix multiplication should suffice:

$$\tilde{\mathbf{S}} = \mathbf{R}_F^t \mathbf{M} \mathbf{R}_F^t \tag{27}$$

where

$$\mathbf{R}_F^t \equiv \mathbf{R}_F^{-1}$$

Expanding the matrix terms out, (27) can be written:

$$\begin{bmatrix} \tilde{S}_{hh} & \tilde{S}_{vh} \\ \tilde{S}_{hv} & \tilde{S}_{vv} \end{bmatrix} = \begin{bmatrix} \cos\Omega & -\sin\Omega \\ \sin\Omega & \cos\Omega \end{bmatrix} \begin{bmatrix} M_{hh} & M_{vh} \\ M_{hv} & M_{vv} \end{bmatrix} \begin{bmatrix} \cos\Omega & -\sin\Omega \\ \sin\Omega & \cos\Omega \end{bmatrix} \tag{28}$$

Since values of $\tan^{-1}$ are between $\pm\pi/2$, values of Ω estimated using (26) will lie between $\pm\pi/4$. Put another way, this means that Ω can only be estimated modulo $\pi/2$ from (26), which is not sufficient. It is straightforward to show that, with an error in Ω of $\pi/2$, the estimate for the corrected scattering matrix from (28) will give:

$$\begin{bmatrix} \tilde{S}_{hh} & \tilde{S}_{vh} \\ \tilde{S}_{hv} & \tilde{S}_{vv} \end{bmatrix} = \begin{bmatrix} -S_{vv} & -S_{hv} \\ S_{vh} & -S_{hh} \end{bmatrix} \tag{29}$$

which is clearly in error. Fortunately, this problem can be identified from the cross-pol terms by comparing measurements before correction (from eq. (16)) and after:

$$\left\langle \tilde{S}_{hv} \tilde{S}_{vh}^* \right\rangle = -\left\langle M'_{hv} M'^*_{hv} \right\rangle$$

and

$$0.25 \left\langle \left(\tilde{S}_{hv} + \tilde{S}_{vh} \right) \left(\tilde{S}_{hv} + \tilde{S}_{vh} \right)^* \right\rangle \neq \left\langle M'_{hv} M'^*_{hv} \right\rangle \tag{30}$$

This test should readily reveal the presence of a $\pi/2$ error in Ω, provided that the cross-pol backscatter S_{hv} (or S_{vh}) is not identically zero. It may be possible to correct for a modulo $\pi/2$ error even in this case, since zero cross-pol backscatter is usually associated with (slightly) rough surface scattering, for which the VV backscatter term is typically greater than or equal to the HH. Thus an examination of the scattering matrix elements may reveal a switch between the two like-polarized measurements due to a $\pi/2$ error in Ω as in (20).

The presence of zero cross-pol backscatter can be determined in advance by examining the symmetrized cross-pol measurement represented by (16). If the phase

change between the two 'corrected' cross-pol estimates is detected using the test represented by equation (30), the procedure to follow should be to add (or subtract) $\pi/2$ from Ω (which means that the largest error in Ω is now $\pm n\pi$), then apply the correction in equation (28) again. It is straightforward to show that, with an error in Ω of π, the estimate for the new corrected scattering matrix will be:

$$\begin{bmatrix} \tilde{S}_{hh} & \tilde{S}_{vh} \\ \tilde{S}_{hv} & \tilde{S}_{vv} \end{bmatrix} = -1 \begin{bmatrix} S_{hh} & S_{vh} \\ S_{hv} & S_{vv} \end{bmatrix} \tag{31}$$

i.e. all scattering matrix elements will be measured correctly, except for an overall phase error of $\pm\pi$. This is largely irrelevant for polarimetric SAR data analysis, in which the cross-products of (31) are of most interest. A phase error of $\pm\pi$ may be significant for analysis of repeat-pass interferometry data, however, in which relative phases between passes are of most interest. In this case, according to Table 1, the problem can be resolved by constraining measurements to night-time periods only, when $\Omega < \pi$.

Summary and Discussion

The effects of Faraday rotation on spaceborne SAR backscatter signatures have been modeled and the detection of Faraday rotation in actual data has been discussed. In the case of single-polarized (HH) measurements, as made by the Japanese JERS-1 satellite, the effects of Faraday rotation should show up primarily as a significant drop in signal-to-noise ratio. It may also be detected as a change in the temporal correlation or in the behavior of certain known scatterers, though this may be difficult to separate from other, scene-dependent changes. In dual-polarized measurements, examination of the relative strength of the nominally 'HH' and 'HV' backscatter measurements and/or the magnitude of the HH-HV correlation coefficient should quickly reveal the presence of Faraday rotation. It may be possible to estimate Ω from the dual-polarized signatures of scatterers which exhibit azimuthal symmetry, such as dense tropical rain forest (at L-Band). For quad-polarized data, in addition to the above indicators, a 180 degree phase change in the argument of the HVVH* term should also quickly reveal the presence of Faraday rotation.

A new technique for estimating Ω and correcting fully polarimetric measurements made by a linearly polarized system has been described. This technique improves on an earlier approach described by [*Bickel and Bates*, 1965] in that it is suited for linear polarization measurements, is computationally simpler, and allows correction for modulo $\pi/2$ errors in the estimate for Ω, provided the cross-pol backscatter is not zero. An approach has been outlined to handle even this eventuality. The resulting correction should be good to within a phase error of $\pm n\pi$. This should not cause problems for L-Band SARs, since the estimated worst-case value for Ω is always significantly less than π (see Table 1). Thus Faraday rotation will not be a problem for LightSAR, which will be capable of fully polarimetric measurements. For P-Band SARs, or even longer wavelengths, it should be possible to avoid larger values of Ω by measuring only at night, when Ω is smallest, to remove any ambiguity.

The new technique for estimating Ω and correcting fully polarimetric measurements presented here should work for any scatterer and be accurate to within a factor of π for scatterers with non-zero cross-pol contribution. To arrive at this conclusion, the reciprocal nature of monostatic radar scattering has been assumed, and the calibration errors due to the radar system itself have been ignored or are assumed to be reliably calibrated out based on prior knowledge or regular system checks. Our experience with other polarimetric SARs

[e.g. *Freeman et al*, 1995] shows these assumptions to be reasonable. The procedures to follow in the presence of radar system channel imbalance errors are discussed in the Appendix.

With the ability to correct for Faraday rotation provided by this technique, a longer wavelength, earth-orbiting SAR becomes feasible. Our calculations show that a P-Band SAR, in a 600 km altitude polar orbit, with a simple linearly polarized reflector antenna and a low-power (100 Watts peak, 5 Watts average) solid-state amplifier with two receive channels, could generate fully polarimetric SAR strip map measurements at an incidence angle of ~35 degrees over a swath width of 50 km at 50 to 100m spatial resolution (on the ground). Such a low-power instrument could easily operate continuously, providing a monitoring capability currently unavailable to earth scientists studying biomass and land cover changes, etc. With the proper choice of a midnight-midday sun-synchronous orbit, earth scientists studying these phenomena could remove uncertainties due to diurnal effects from their observations, and study seasonal effects with a guaranteed revisit period of, say, one month.

It can also be postulated that a new type of measurement technique for ionospheric phenomena could arise from a low earth orbiting P-Band SAR such as the one outlined above. From equation (2), and in a similar fashion to the ground-based Faraday polarimeter technique described in [*Titheridge*, 1972], the procedure for extracting the Faraday rotation angle Ω from polarimetric backscatter data could be used to continuously generate spatial maps of electron content at, say, 500 m intervals, over a 50 km wide strip as the orbiter proceeds along its path. This would allow the study of the spatial structure of certain ionospheric phenomena. Such measurements would complement existing, ground-based measurements, such as those provided by Faraday polarimeters, incoherent radar scatter data, radio tomographic techniques and ionosondes. These techniques can provide extremely good temporal coverage and vertical profiling, but are necessarily localized in their nature. The new approach described here would provide maps of electron content in otherwise inaccessible areas, and on a global scale, albeit at rather infrequent intervals.

Acknowledgments

Part of the research described in this paper was carried out by the Jet Propulsion Laboratory, California Institute of Technology, under a contract with the National Aeronautics and Space Administration. The authors would like to thank the LightSAR Project and the Advanced Radar Technology Program for their support of this work and Scott Hensley, Simon Yueh and Son Nghiem for some helpful discussions on this topic.

Appendix: Faraday Rotation and Channel Imbalance

Based on our experience with spaceborne SAR polarimetric data acquired during the SIR-C missions [*Freeman et al*, 1995] it is reasonable to assume that a SAR system can be built with negligible levels of cross-talk, and relatively good gain stability, but that the channel amplitude and phase imbalances may vary over time, or with the mode of operation. This means that (ignoring additive noise) a more realistic model for the polarimetric measurements may be given by:

$$\begin{bmatrix} M_{hh} & M_{vh} \\ M_{hv} & M_{vv} \end{bmatrix} = \begin{bmatrix} 1 & 0 \\ 0 & f_1 \end{bmatrix} \begin{bmatrix} \cos\Omega & \sin\Omega \\ -\sin\Omega & \cos\Omega \end{bmatrix} \begin{bmatrix} S_{hh} & S_{vh} \\ S_{hv} & S_{vv} \end{bmatrix} \begin{bmatrix} \cos\Omega & \sin\Omega \\ -\sin\Omega & \cos\Omega \end{bmatrix} \begin{bmatrix} 1 & 0 \\ 0 & f_2 \end{bmatrix} \tag{A1}$$

where the complex term f_1 represents the receive H-V channel amplitude and phase imbalance and f_2 represents the transmit H-V channel amplitude and phase imbalance. Comparing eq. (A1) with eq. (4) it can be seen that we have ignored the system noise, the overall system gain term A and, further, the off-diagonal terms in **R** and **T**, which represent the system cross-talk, have been set to zero.

To calibrate the measurements represented by (A1) it is necessary to first determine the three unknowns: f_1, f_2 and Ω. Expanding (A1) and invoking backscatter reciprocity, we obtain an updated version of eq. (8), i.e.:

$$M_{hh} = S_{hh}\cos^2\Omega - S_{vv}\sin^2\Omega \tag{A2a}$$

$$M_{vh} = f_2\left[S_{hv} + \left(S_{hh} + S_{vv}\right)\sin\Omega\cos\Omega\right] \tag{A2b}$$

$$M_{hv} = f_1\left[S_{hv} - \left(S_{hh} + S_{vv}\right)\sin\Omega\cos\Omega\right] \tag{A2c}$$

$$M_{vv} = f_1 f_2\left[S_{vv}\cos^2\Omega - S_{hh}\sin^2\Omega\right] \tag{A2d}$$

Forming the cross-product between the two cross-pol measurements in (A2b) and (A2c), we obtain,

$$\left\langle M_{hv}M_{vh}^*\right\rangle = f_1 f_2^*\left[S_{hv}S_{hv}^* - \left(S_{hh}S_{hh}^* + S_{vv}S_{vv}^* + 2\mathrm{Re}\left\{S_{vv}S_{vv}^*\right\}\right)\sin^2\Omega\cos^2\Omega\right] \tag{A3}$$

The term in square brackets on the right-hand side of (A3) is a real number, which can take positive or negative values. This is the same as the expression in (15) whose phase transitions were plotted in Figure 6. Thus:

$$\arg\left\{\left\langle M_{hv}M_{vh}^{*}\right\rangle\right\} = \arg\left\{f_1 f_2^{*}\right\} \pm n\pi \tag{A4}$$

where n = 0 if the term in square brackets is positive, and n = 1 if it is negative. Put another way, it is possible to recover the relative phase between f_1 and f_2 to within π, depending on the sign of the term in square brackets.

It is straightforward to show that, provided (14) holds, i.e. that like-and cross-pol backscatter terms are uncorrelated,

$$\frac{\left\langle M_{hv}M_{hv}^{*}\right\rangle}{\left\langle M_{vh}M_{vh}^{*}\right\rangle} = \frac{|f_1|^2}{|f_2|^2} \tag{A5}$$

Thus the relative amplitude between f_1 and f_2 can be recovered using (A5). Combining the two, the estimated value for the ratio is:

$$\left(\frac{\hat{f}_1}{f_2}\right) = \pm \frac{f_1}{f_2} \tag{A6}$$

Next, if we form the symmetrized cross-pol measurement,

$$M_{hv}^{'} = 0.5\left(M_{hv} + \left(\frac{\hat{f}_1}{f_2}\right)M_{vh}\right) \equiv f_1 S_{hv} \text{ if } \left(\frac{\hat{f}_1}{f_2}\right) = \frac{f_1}{f_2}$$

$$\equiv -f_1\left(S_{hh} + S_{vv}\right)\sin\Omega\cos\Omega \text{ if } \left(\frac{\hat{f}_1}{f_2}\right) = -\frac{f_1}{f_2} \tag{A7}$$

If the sign of the estimated ratio is in error by π, then:

$$\left\langle M_{hh}M_{hv}^{'*}\right\rangle \neq 0$$

unless $\Omega = n\pi/2$, n integer, in which case it can also be seen that:

$$\left\langle M'_{hv} M'^{*}_{hv} \right\rangle = 0$$

Thus, provided the cross-pol backscatter is not zero, it should be possible to determine when the phase of the estimated ratio has an error of π. Again, experience with SIR-C data revealed that the argument of (f_1/f_2) varied very little, so the scenario outlined above should easily be detected as a sudden change in this value from previously determined values or by comparing with vales obtained during night-time passes, when Ω should be small.

Once (f_1/f_2) is completely determined, the cross-pol measurement can be symmetrized as in (A7), and a factor (f_1/f_2) applied to (A2d) to give:

$$M_{hh} = S_{hh}\cos^2\Omega - S_{vv}\sin^2\Omega \tag{A8a}$$

$$M'_{vh} = f_1\left[S_{hv} + \left(S_{hh} + S_{vv}\right)\sin\Omega\cos\Omega\right] \tag{A8b}$$

$$M_{hv} = f_1\left[S_{hv} - \left(S_{hh} + S_{vv}\right)\sin\Omega\cos\Omega\right] \tag{A8c}$$

$$M'_{vv} = \left(f_1\right)^2\left[S_{vv}\cos^2\Omega - S_{hh}\sin^2\Omega\right] \tag{A8d}$$

which is similar to (A2), except for the presence of the factor f_1. In a similar fashion to [*Freeman et al*, 1992], the transmit channel imbalance f_2 has been removed to leave only f_1, the receive channel imbalance, in (A8). This is easier to calibrate using prior measurements and/or reference signals fed into the system receive chain. Note that (A8) consists of 4 equations in 5 unknowns - it is not possible to solve for any one of these without further knowledge of the scattering matrix values or f_1. If f_1 is known, (A8b-d) can be corrected and the steps outlined for correction of Faraday rotation in section 5.3 can be followed.

References

Bickel, S. H. and Bates, R. H. T., Effects of Magneto-Ionic Propagation on the Polarization Scattering matrix, Proc. IRE, Vol. 53, No. 8, pp. 1089-1091, 1965.

Bowles, K. L. et al, "Profiles of Electron Density over the Magnetic Equator obtained using the Incoherent Scatter Technique", National Bureau of Standards Technical Note 169, March 1963.

Chu, T. S and Lenzing, H. F., "Ionosphere-induced Cross Polarization of Circularly Polarized UHF Propagation", IEEE Trans. on Antennas and Propagation, Vol. 39, No. 11, pp. 1644-1647, November 1991.

Daniell, R. E., Jr., Brown, L. D., Strickland, D. J., Barnes, R. P., Klobuchar, J. A. and Thompson, R. H., "Traveling Ionospheric Disturbances Observed in Digitized Polarimeter Data", Radio Science, Vol. 31, No. 6, pp. 1589-1598, November-December 1996.

Dobson, M. C., Ulaby, F. T., LeToan, T., Beaudoin, A., Kasischke, E. S. and Christiansen, "Dependence of radar backscatter on conifer forest biomass", IEEE Trans. on Geoscience and Remote Sensing, Vol. 30, pp. 403-411, 1992.

Evans, J. V. and Hagfors, T., "Radar Astronomy", publ. McGraw-Hill, New York, 1968.

Evans, D. (ed.), "Spaceborne Synthetic Aperture Radar: Current Status and Future Directions", A report to the Committee on Earth Sciences, National Research Council, NASA Technical Memorandum 4679, April 1995.

Ezquer, R. G., de Adler, N. O., Heredia, T., "Predicted and measured total electron content at both peaks of the equatorial anomaly", Radio Science, Vol. 29, No. 4, pp. 831-838, July-August 1994.

Ezquer, R. G., del Oviedo, R., and Jadur, C. A., "Ionospheric predictions for South America latitudes", Radio Science, Vol. 31, No. 2, pp. 381-388, March-April 1996.

Freeman, A., van Zyl, J. J., Klein, J. D., Zebker, H. A. and Shen, Y., Calibration of Stokes and scattering matrix format polarimetric SAR data, IEEE Trans. on Geoscience and Remote Sensing, Vol. 30, No. 3, pp. 531-539, May 1992.

Freeman, A., "SAR Calibration: An Overview", IEEE Trans. on Geoscience and Remote Sensing, Vol. 30, pp. 1107-1121, November 1992.

Freeman, A., Cruz, J., Alves, M., Chapman, B., S. Shaffer and Turner, E., SIR-C Data Quality and Calibration Results, IEEE Trans. Geosci. Remote Sensing, vol. 33, no. 4, July 1995.

Freeman, A. and Durden, S., "A Three-Component Scattering Model for Polarimetric SAR Data", accepted for publication, IEEE Trans. on Geoscience and Remote Sensing, 1997

Gail, W. B., 1995, "Effect of Faraday rotation on Polarimetric SAR," in press, IEEE Trans. on Aerospace and Electronic Systems., Vol. 34, No. 1, January 1998.

Gail, W. B., 1993, "A Simplified Calibration Technique for Polarimetric Radars," Proc. IGARSS '93, Tokyo, Japan, 1993, Vol. II, pp. 377-379.

Garriott, O. K., Smith, F. L., and Yuen, P. C., "Observations of Ionospheric Electron Content using a Geostationary Satellite", Planet. Space Sci., Vol. 13, pp. 829-838, 1965.

Hunsucker, R. D., "Auroral and Polar-Cap Ionospheric Effects on Radio Propagation", IEEE Trans. on Antennas and Propagation, Vol. 40, No. 7, pp. 818-828, July 1992.

Ishimaru, A., Kuga, Y. and Liu, J., "Study of Ionospheric/Tropospheric Effects on SAR Operation for the JPL/NASA Advanced Radar Technology Program", December 1997.

Kutuza, B. G., Kalinkevitch, A. A., Ephimov, A. I. , Vostrov, E. A. and Dzenkevitch, A. B., "Application of SAR operating at P-Band for Space Experiments", Proc. EUSAR '96, European Conference on Synthetic Aperture Radar, Konigswinter, Germany, pp. 309-313, 1996.

Le Toan, T., Beaudoin, A., Riom, J. and Guyon, D., "Relating forest biomass to SAR data", IEEE Trans. on Geoscience and Remote Sensing, Vol. 30, pp. 403-411, 1992.

Nghiem, S. V., Yueh, S. H., Kwok, R. and Li. F. K., "Symmetry Properties in Polarimetric Remote Sensing", Radio Science, Vol. 27, No. 5, pp. 693-711, September-October 1992.

Quegan, S. and Lamont, J., "Ionospheric and Tropospheric effects on synthetic aperture radar performance", Int. J. Remote Sensing, Vol. 7, No. 4, pp. 525-539, 1986.

Rignot, E. J., Zimmermann, R. and van Zyl, J. J., "Spaceborne Applications of P-Band Imaging Radars for Measuring Forest Biomass", IEEE Trans. on Geoscience and Remote Sensing, Vol. 33, No. 5, pp. 1162-1169, September 1995.

Rosen, P., 1992, "Study of Faraday rotation effects on P-Band polarimetric spaceborne SAR", JPL interoffice memorandum #3343-92-72, August 1992.

Thompson, A. R., Moran, J. M., and Swenson, G. W., "Interferometry and Synthesis in Radio Astronomy", publ. John Wiley & Sons, 1986.

Titheridge, J. E., "Determination of Ionospheric Electron Content from the Faraday Rotation of Geostationary Satellite Signals", Planet. Space Sci., Vol. 20, pp. 353-369, 1972.

K. C Yeh and C. H Liu, "Theory of ionosphere waves", Academic Press, NY 1972.